Viscosity kernel of molecular fluids: Butane and polymer melts

R. M. Puscasu* and B. D. Todd†
Centre for Molecular Simulation, Swinburne University of Technology, P.O. Box 218, Hawthorn, Victoria 3122, Australia

P. J. Daivis‡
Applied Physics, School of Applied Sciences, RMIT University, G.P.O. Box 2476, Melbourne, Victoria 3001, Australia

J. S. Hansen§
DNRF Centre "Glass and Time," IMFUFA, Roskilde University, P.O. Box 260, DK-4000 Roskilde, Denmark

(Received 11 February 2010; revised manuscript received 27 April 2010; published 9 July 2010)

The wave-vector dependent shear viscosities for butane and freely jointed chains have been determined. The transverse momentum density and stress autocorrelation functions have been determined by equilibrium molecular dynamics in both atomic and molecular hydrodynamic formalisms. The density, temperature, and chain length dependencies of the reciprocal and real-space viscosity kernels are presented. We find that the density has a major effect on the shape of the kernel. The temperature range and chain lengths considered here have by contrast less impact on the overall normalized shape. Functional forms that fit the wave-vector-dependent kernel data over a large density and wave-vector range have also been tested. Finally, a structural normalization of the kernels in physical space is considered. Overall, the real-space viscosity kernel has a width of roughly 3–6 atomic diameters, which means that generalized hydrodynamics must be applied in predicting the flow properties of molecular fluids on length scales where the strain rate varies sufficiently in the order of these dimensions (e.g., nanofluidic flows).

DOI: 10.1103/PhysRevE.82.011801 PACS number(s): 61.25.H−, 66.20.Cy, 66.20.Gd, 61.20.Ja

I. INTRODUCTION

Because of their technological relevance, polymer solutions and melts are the subject of intense study. In recent years there has been considerable interest in molecular based theories and simulations of thermodynamic and transport properties of such systems. Though experimental shrinking of molecular based fluidic devices from the micron regime to the nanometer regime has shown remarkable developments over the last decade, there are still many fundamental challenges to be addressed [1,2]. Since extremely small volumes are involved, molecular systems are very difficult to handle and manipulate using conventional technologies. Therefore, modeling and simulation techniques are useful tools to study molecular structures on such length scales. Many simulations of nanofluids, in particular equilibrium molecular-dynamics (EMD) and nonequilibrium molecular-dynamics (NEMD) simulations, have been performed in the late 1980s early 1990s [3,4] and more extensively in recent years [5]. However, in most of these simulations the stress was only treated as being dependent on the local strain rate. Newton's law of viscosity breaks down on very small length scales and even exhibits singularities at points where the strain rate is zero [6–9]. Todd *et al.* [10,11] recently shown that for flow fields with nonconstant gradients in the strain rate over the width of the real-space viscosity kernels, nonlocality plays a significant role. In the case of planar Couette and Poiseuille flows, the inclusion of the nonlocal viscosity kernel will give exactly the same predictions as classical hydrodynamics, which assumes a constant local viscosity [10]. However, for more general cases, the stress cannot be thought of as a local function of the strain rate, but the entire strain rate distribution in the system. Such a nonlocal constitutive equation that allows for spatial and temporal nonlocality for a homogeneous fluid can be expressed as [12,13]

$$P_{xy}(\mathbf{r},t) = -\int_0^t \int_{-\infty}^{\infty} \eta(\mathbf{r}-\mathbf{r}',t-t')\,\dot{\gamma}(\mathbf{r}',t')d\mathbf{r}'dt', \quad (1)$$

where $P_{xy}(\mathbf{r},t)$ is the (x,y) off-diagonal component of the pressure tensor, $\dot{\gamma}(\mathbf{r}',t')$ is the shear strain rate, and $\eta(\mathbf{r}-\mathbf{r}',t-t')$ is the nonlocal viscosity kernel at position $\mathbf{r}$ and time t. In the situation where the strain rate is constant in time and only varies with respect to the spatial coordinate y, Eq. (1) reduces to

$$P_{xy}(y) = -\int_{-\infty}^{\infty} \eta(y-y')\,\dot{\gamma}(y')dy'. \quad (2)$$

Highly confined systems exhibit large variations in the strain rate with position in the vicinity of the wall. Therefore a nonlocal constitutive equation is expected to be necessary for an adequate description of flow in such systems [6].

The wave-vector-dependent shear viscosity in Eq. (2) for a variety of simple atomic fluids has already been discussed by several authors [12,14,15]. A more extensive analysis of the wave-vector-dependent shear viscosity for monatomic and diatomic fluids has been carried out in our other publication [16]. Molecular fluids have received less attention with very few results on nonlocal transport coefficients. Palmer [17] reported the transverse current autocorrelation

*rpuscasu@swin.edu.au
†btodd@swin.edu.au
‡peter.daivis@rmit.edu.au
§jesperschmidthansen@gmail.com

functions for Lennard-Jones fluids, liquid carbon dioxide, and the TIP4P model of water in the small wave-vector region. Bertolini *et al.* [18] reported the density, longitudinal, and transverse currents for water, modeled by a TIP4P potential in the atomic and molecular formalism for three wave vectors $(0.288, 0.498, 0.705\ \text{Å}^{-1})$ and the stress autocorrelation functions (ACFs) at the same value of wave vectors and at zero wave vector for 245 K. More recently a modified collective mode approach has been applied by Omelyan *et al.* [19] to TIP4P water. They reproduced the wave-vector and frequency dependent shear viscosity for this model using a relatively small number of modes.

Generally, molecular hydrodynamic theories may be framed in atomic or molecular formalisms [20–24] which only agree in the limit of zero frequency and zero wave vector. For simple atomic fluids [15] and water [17,18] the wave-vector dependences of bulk and shear viscosities were qualitatively similar to those of hard spheres [12] which confirms that the hard sphere model is a very good approximation for dense liquid properties that depend on the liquid structure. The ACFs for water [18] and chlorine [16] were essentially equal in both atomic and molecular formalisms.

The aim of this work is to extract the homogeneous nonlocal viscosity kernel for complex molecular fluids over a large range of wave vectors, densities, and temperatures. In the paper we report results for butane and long linear chains. The molecular dynamics results allow us to propose a functional form for the nonlocal viscosity kernel in reciprocal space that fits the data over the considered domain of state points. The inverse Fourier transformed functions can then be used to compute the real space kernels. Ultimately, the identified viscosity kernel allows one to predict the flow profile for confined molecular fluids.

The remainder of this paper is organized as follows: in Sec. II we briefly review the theoretical concepts. In Secs. II A and II B the atomic and molecular hydrodynamic expressions for the wave-vector-dependent momentum density and stress are introduced. In Sec. II C the expressions for the complex wave-vector and frequency dependent viscosity are given. In Sec. III we describe our models and simulation conditions. In Sec. IV we present results including the reciprocal and real space kernels for our molecular systems. A structural normalization of the real space kernels that accounts for structural properties is also considered in this section. In Sec. V we draw conclusions and make a few closing remarks.

II. METHOD

A. Wave-vector-dependent momentum densities

The mass and momentum densities in the atomic representation for a molecular fluid are defined in real space as [25]: $\rho(\mathbf{r},t)=\sum_{i=1}^{N_m}\sum_{\alpha=1}^{N_s} m_{i\alpha}\delta(\mathbf{r}-\mathbf{r}_{i\alpha})$ and $\mathbf{J}^A(\mathbf{r},t)=\rho(\mathbf{r},t)\mathbf{v}(\mathbf{r},t)=\sum_{i=1}^{N_m}\sum_{\alpha=1}^{N_s}\mathbf{p}_{i\alpha}(t)\delta(\mathbf{r}-\mathbf{r}_{i\alpha})$ where the inner summation extends over the number of interaction sites N_s in a molecule and the outer summation extends over the number of molecules N_m in the system. In general, N_s, depends on the molecule index i for a multicomponent system, but in our systems N_s is constant and the atoms are assumed to have identical masses, namely, $m_{i\alpha}$. The Fourier transform of the mass density is $\tilde{\rho}(\mathbf{k},t)=\sum_{i=1}^{N_m}\sum_{\alpha=1}^{N_s} m_{i\alpha}e^{i\mathbf{k}\cdot\mathbf{r}_{i\alpha}}$, with $\mathbf{k}$ being the wave vector, and the Fourier transform of the momentum density is

$$\tilde{\mathbf{J}}^A(\mathbf{k},t)=\sum_{i=1}^{N_m}\sum_{\alpha=1}^{N_s}\mathbf{p}_{i\alpha}(t)e^{i\mathbf{k}\cdot\mathbf{r}_{i\alpha}}. \tag{3}$$

For molecules composed of N_s atoms we can define the molecular mass as $M_i=\sum_{\alpha=1}^{N_s} m_{i\alpha}$, the position of the molecular center of mass as $\mathbf{r}_i=\sum_{\alpha=1}^{N_s} m_{i\alpha}\mathbf{r}_{i\alpha}/M_i$ and momentum of the molecule i as $\mathbf{p}_i=\sum_{\alpha=1}^{N_s}\mathbf{p}_{i\alpha}$. This means that the molecular momentum density can be written in reciprocal space as

$$\tilde{\mathbf{J}}^M(\mathbf{k},t)=\sum_{i=1}^{N_m}\mathbf{p}_i(t)e^{i\mathbf{k}\cdot\mathbf{r}_i}. \tag{4}$$

The reciprocal and real space expressions of mass and momentum densities for a molecular fluid has been discussed in more detail by Todd and Daivis [25].

B. Wave-vector-dependent pressure tensor

The molecular pressure is the pressure calculated using the intermolecular forces and the molecular center of mass momenta. The atomic pressure on the other hand includes all atomic momenta and all interatomic forces and constraint forces. The wave-vector-dependent atomic pressure tensor for a polymer system composed of N_m molecules and N_s sites per molecule is defined as

$$\begin{aligned}\tilde{\mathsf{P}}^{AFJC}(\mathbf{k},t)=&\sum_{i=1}^{N_m}\sum_{\alpha=1}^{N_s}\frac{\mathbf{p}_{i\alpha}\mathbf{p}_{i\alpha}}{m_{i\alpha}}e^{i\mathbf{k}\cdot\mathbf{r}_{i\alpha}}\\&-\frac{1}{2}\sum_{i=1}^{N_m}\sum_{\alpha=1}^{N_s}\sum_{j\neq i}^{N_m}\sum_{\beta=1}^{N_s}\mathbf{r}_{i\alpha j\beta}\mathbf{F}_{i\alpha j\beta}g(i\mathbf{k}\cdot\mathbf{r}_{i\alpha j\beta})e^{i\mathbf{k}\cdot\mathbf{r}_{i\alpha j\beta}}\\&-\sum_{i=1}^{N_m}\sum_{\alpha=1}^{N_s-2}\sum_{\beta=\alpha+2}^{N_s}\mathbf{r}_{i\alpha i\beta}\mathbf{F}_{i\alpha i\beta}g(i\mathbf{k}\cdot\mathbf{r}_{i\alpha i\beta})e^{i\mathbf{k}\cdot\mathbf{r}_{i\alpha i\beta}}\\&+\sum_{i=1}^{N_m}\sum_{\alpha=1}^{N_s}\mathbf{r}_{i\alpha}\mathbf{F}_{i\alpha}^{C}g(i\mathbf{k}\cdot\mathbf{r}_{i\alpha})e^{i\mathbf{k}\cdot\mathbf{r}_{i\alpha}},\end{aligned} \tag{5}$$

where $\mathbf{F}_{i\alpha j\beta}$ is the LJ force acting on site α of molecule i due to site β of molecule j and $\mathbf{F}_{i\alpha}^{C}$ is the total bond constraint force on site α of molecule i. $\mathbf{r}_{i\alpha j\beta}=\mathbf{r}_{j\beta}-\mathbf{r}_{i\alpha}$ is the minimum image separation of site α of molecule i from site β of molecule j. $g(i\mathbf{k}\cdot\mathbf{r})$ are the Fourier transforms of the Irving-Kirkwood operators [26], where $g(x)=(e^x-1)/x=\sum_{n=0}^{\infty}(x)^n/(n+1)!$, with $x=i\mathbf{k}\cdot\mathbf{r}_{i\alpha j\beta}$, $x=i\mathbf{k}\cdot\mathbf{r}_{i\alpha i\beta}$, and $x=i\mathbf{k}\cdot\mathbf{r}_{i\alpha}$, respectively. The second and third terms in Eq. (5) represent the intermolecular and intramolecular contributions to the pressure tensor, respectively.

For butane, a torsional or dihedral force component $\mathbf{F}^D$ should be also included in the pressure tensor so that

$$\tilde{\mathsf{P}}^{A^{Butane}}(\mathbf{k},t) = \sum_{i=1}^{N_m}\sum_{\alpha=1}^{N_s}\frac{\mathbf{p}_{i\alpha}\mathbf{p}_{i\alpha}}{m_{i\alpha}}e^{i\mathbf{k}\cdot\mathbf{r}_{i\alpha}} - \frac{1}{2}\sum_{i=1}^{N_m}\sum_{\alpha=1}^{N_s}\sum_{j\neq i}^{N_m}\sum_{\beta=1}^{N_s}\mathbf{r}_{i\alpha j\beta}\mathbf{F}_{i\alpha j\beta}g_{i\alpha j\beta}(\mathbf{k})e^{i\mathbf{k}\cdot\mathbf{r}_{i\alpha j\beta}} + \sum_{i=1}^{N_m}\sum_{\alpha=1}^{N_s}\mathbf{r}_{i\alpha}\mathbf{F}^{D}_{i\alpha}g_{i\alpha}(\mathbf{k})e^{i\mathbf{k}\cdot\mathbf{r}_{i\alpha}} + \sum_{i=1}^{N_m}\sum_{\alpha=1}^{N_s}\mathbf{r}_{i\alpha}\mathbf{F}^{C}_{i\alpha}g_{i\alpha}(\mathbf{k})e^{i\mathbf{k}\cdot\mathbf{r}_{i\alpha}}, \quad (6)$$

where $\mathbf{F}^{C}_{i\alpha}$ is the intramolecular constraint forces.

The pressure tensor in the molecular representation is defined for both systems as

$$\tilde{\mathsf{P}}^{\mathsf{M}}(\mathbf{k},t) = \sum_{i=1}^{N_m}\frac{\mathbf{p}_i\mathbf{p}_i}{M_i}e^{i\mathbf{k}\cdot\mathbf{r}_i} - \frac{1}{2}\sum_{i=1}^{N_m}\sum_{j\neq i}^{N_m}\mathbf{r}_{ij}\mathbf{F}^{inter}_{ij}g_{ij}(\mathbf{k})e^{i\mathbf{k}\cdot\mathbf{r}_{ij}}, \quad (7)$$

where $\mathbf{F}^{inter}_{ij}$ represents the intermolecular force. $g_{ij}(\mathbf{k}) = (e^{i\mathbf{k}\cdot\mathbf{r}_{ij}}-1)/i\mathbf{k}\cdot\mathbf{r}_{ij} = \Sigma_{n=0}^{\infty}(i\mathbf{k}\cdot\mathbf{r}_{ij})^n/(n+1)!$. $\mathbf{r}_{ij}=\mathbf{r}_j-\mathbf{r}_i$ is the minimum image separation of the center of mass of molecule i from the center of mass of molecule j. The momenta appearing in these equations, $\mathbf{p}_{i\alpha}$, $\mathbf{p}_i$, are the momenta appearing in the respective atomic and molecular equations of motion [Eqs. (17) and (18)]. The atomic pressure tensor is symmetric at all times by definition. Although the time averaged molecular and atomic pressure tensor should be identical, the molecular pressure tensor may not be symmetric instantaneously. We must note also that the contribution of the internal molecular forces, such as constraint and dihedral forces, to the molecular pressure is zero because the sum of an internal force over all sites within molecules is zero. A more detailed derivation of atomic and molecular wave-vector-dependent pressure tensor can be found in [20,23,27].

C. Wave-vector- and frequency-dependent viscosity

In what follows we present expressions for the wave-vector- and frequency-dependent viscosities derived only for the atomic representation. Because the molecular stress tensor is not symmetric instantaneously the formulation of correlation function expressions is more complex and will not be considered in this paper.

The wave-vector- and frequency-dependent viscosity can be evaluated by using two different expressions in terms of the Fourier-Laplace transform of the transverse momentum density ACF, $C_\perp(\mathbf{k},t)$, and the Fourier-Laplace transform of the stress tensor autocorrelation function, $N(\mathbf{k},t)$ [13]. We define the Fourier-Laplace transform (one-sided Fourier transform) as $\mathcal{L}[f(t)]=\tilde{f}(\omega)=\int_0^\infty f(t)e^{-i\omega t}dt$. For the sake of simplicity of notation and consistency with the notation used in previous publications, in what follows, we drop the tilde sign over correlation functions and keep the tilde notation over the Fourier-Laplace transformed correlation functions only. If we set the wave vector $(0,k_y,0)$ in reciprocal space and let J_x be the component of the momentum density in the x direction, the expression for the wave-vector- and frequency-dependent viscosity in terms of $\tilde{C}_\perp(k_y,\omega)$ takes the form [13]

$$\tilde{\eta}(k_y,\omega) = \frac{\rho}{k_y^2}\frac{C_\perp(k_y,t=0)-i\omega\tilde{C}_\perp(k_y,\omega)}{\tilde{C}_\perp(k_y,\omega)}, \quad (8)$$

where ρ is the atomic mass density of the fluid and $\tilde{C}_\perp(k_y,\omega)$ is the Laplace transform of the ensemble averaged transverse momentum density ACF $C_\perp(k_y,t)$, which is defined as

$$C_\perp(k_y,t) = \frac{1}{V}\langle J_x(k_y,t)J_x(k_y,t=0)\rangle, \quad (9)$$

where V is the simulation volume. The integral of the transverse momentum density ACF is given as

$$I_{C_\perp}(k_y,t) = \int_0^t C_\perp(k_y,t')dt'. \quad (10)$$

The zero time value of $C_\perp(k_y,t=0)$ for an atomic fluid in the thermodynamic limit is

$$C_\perp(k_y,t=0) = \rho k_B T \quad (11)$$

and k_B is Boltzmann's constant. The theoretical value of $C_\perp(k_y,t=0)=\rho k_B T$ for an atomic fluid obtained from a canonical ensemble average in the thermodynamic limit differs slightly from the theoretical value in the simulated isokinetic ensemble given by $C_\perp(k_y,t=0)=\rho k_B T(1-4N_sN_m/3)$ because the total peculiar kinetic energy and three components of the momenta are constants of the motion in our simulations. For a molecular fluid with constrained bonds, we must also account for the internal bond constraints in deriving a relationship between the zero time value of the atomic momentum density ACF and the temperature. This point is discussed further in the results section. To ensure numerical consistency of our results, we use the simulated value of $C_\perp(k_y,t=0)$ rather than Eq. (11) in our calculations of the wave-vector-dependent viscosity.

The expression for the wave-vector- and frequency-dependent viscosity in terms of the ACF of the shear stress $N(k_y,t)$ takes the form

$$\tilde{\eta}(k_y,\omega) = \frac{\tilde{N}(k_y,\omega)}{C_\perp(k_y,t=0)/\rho k_B T - k^2\tilde{N}(k_y,\omega)/i\omega\rho}, \quad (12)$$

where

$$\tilde{N}(k_y,\omega) = \frac{1}{Vk_BT}\mathcal{L}[\langle P_{xy}(k_y,t)P_{xy}(k_y,t=0)\rangle], \quad (13)$$

and again we point out that Eq. (12) is only valid in the atomic representation. In the zero wave-vector limit, a generalization of the Green-Kubo expression for the shear viscosity for an isotropic fluid allows the transverse momentum flux to be in an arbitrary direction rather than along a coordinate axis and can be written in terms of the stress tensor as [28,29]

$$\eta = \frac{V}{10k_BT}\int_0^\infty dt\langle \mathsf{P}^{os}(t):\mathsf{P}^{os}(0)\rangle, \tag{14}$$

where the *os* superscript denotes the traceless symmetric part of the stress tensor $\mathsf{P}^{os}(t)=\frac{1}{2}[\mathsf{P}(t)+\mathsf{P}^T(t)]-\frac{1}{3}tr[\mathsf{P}(t)]\mathbf{1}$. Equation (14) is valid for both atomic and molecular representations.

The integral of the shear stress ACF can be written as

$$I_N(k_y,t) = \int_0^t N(k_y,t')dt', \tag{15}$$

which converges to the Green-Kubo viscosity for zero wave vector and to zero at the nonzero wave-vector values. This is used as a direct computational verification of the statement that the zero-frequency limit of the function $\tilde{N}(\mathbf{k},\omega)$ is zero for all nonzero wave vectors and demonstrates why neither substitution of $\omega=0$ into Eq. (12) nor evaluation of Eq. (13) at nonzero wave vector yields the zero-frequency wave-vector-dependent viscosity [13]. For the nonzero wave-vector viscosity Eq. (8) must be used.

III. SIMULATION

A. Model

Our simulation is based on the Edberg, Evans, and Morriss algorithm [22,30,31] with an improved cell neighbor list construction algorithm [32]. To simulate butane we have used the united atom model by Ryckaert and Bellemans [29,33,34]. In this model each molecule is composed of $N_s=4$ sites of mass 2.411×10^{-23} g which represent methyl groups. The distance between neighboring sites is fixed to 1.53 Å and bond angles are fixed to 109.47° by a next-nearest-neighbor constraint. A dihedral potential that depends on the dihedral angle ϕ acts between each pair of methyl groups. We use a simple truncated cosine power series for the dihedral potential. We note here that while the semiflexible Ryckaert and Bellemans model reproduces the equilibrium properties of *n*-alkanes satisfactorily, it does not correctly generate all the transport coefficients [22]. More sophisticated models have to be employed in order to get a better agreement with experiment [35–40].

The molecular model that we have chosen to represent polymer molecules is the freely jointed Lennard-Jones (LJ) chain (FJC) model. Each molecule in this model consists of N_s sites of equal mass $m_{i\alpha}$ which interact via a truncated $(r_c=2^{1/6})$ and shifted LJ interaction [known as the Weeks-Chandler-Andersen (WCA) interaction], Eq. (16) [41], joined by rigidly constrained bonds of length $l=\sigma$. LJ interactions in this model can occur between any two different sites except those connected by a bond,

$$\Phi_{ij}(r_{ij}) = \begin{cases} 4\epsilon\left[\left(\dfrac{\sigma}{r_{ij}}\right)^{12} - \left(\dfrac{\sigma}{r_{ij}}\right)^{6}\right] - \Phi_c, & r_{ij} < r_c \\ 0, & r_{ij} \geq r_c, \end{cases} \tag{16}$$

where r_{ij} is the interatomic separation, ϵ is the potential well depth, and σ is the value of r_{ij} at which the unshifted potential is zero. The shift Φ_c is the value of the unshifted potential at the cutoff $r_{ij}=r_c$ and is introduced to eliminate the discontinuity in the potential energy.

TABLE I. Simulation details.

	Butane	FJC/FENE
Site number density, ρ	1.676, 1.46	0.84
Temperature, T	4.05, 3.79	1
Number of molecules, N_m	108, 864	108, 864
Number of sites, N_s	4	10, 20, 50
Bond length, l	0.39	1
LJ cutoff, r_c	2.5	$2^{1/6}$

We have also studied the chain length dependence of the viscosity kernel. A series of three different molecular sizes was studied, consisting of 10, 20, and 50-site molecules. The system size was 108 and 864 molecules. The molecular temperature was $T=1.0$ and the reduced atomic (site) number density was $\rho=0.84$, where we note that the atomic number density is equal to the atomic mass density in reduced units for our system because all particles have the same mass. The state point was chosen to correspond to previous studies [42–44] of chain dynamics. These parameters remained constant through this series of simulations. The values of the relevant simulation parameters are summarized in Table I. All quantities in this paper are reported in terms of reduced units which are relative to the Lennard-Jones parameters. The conversion from real units to reduced units gives: reduced length $r^*=r/\sigma$, reduced density $\rho^*=\rho/\sigma^3$, reduced temperature $T^*=k_BT/\epsilon$, reduced time $t^*=t/(\sigma(m/\epsilon)^{1/2}$, reduced pressure $\mathsf{P}^*=\mathsf{P}(\sigma^3/\epsilon)$, reduced energy $E^*=E/\epsilon$, and reduced viscosity $\eta^*=\eta\sigma^2/\sqrt{(m\epsilon)}$. For the remainder of this paper the asterisk is dropped.

B. Equations of motion

We conduct the simulations using a fifth-order Gear algorithm [45,46] with an integration time step of $\delta t=0.002$. The equations of motion (EOM) for a molecular fluid can be given in either the atomic or molecular formalism. In fact, the molecular version of the homogeneous isothermal EOM with a molecular thermostat at equilibrium are similar to the atomic EOM with a molecular thermostat provided that all of the relevant forces are included [25]. When an atomic thermostat is formulated artifacts are generated, however, this is not the case here as all our simulations are performed at constant molecular temperature which is a common practice in simulation of molecular fluids including polymeric fluids. The thermostatted EOM for polymer melts are given by [25]

$$\dot{\mathbf{r}}_{i\alpha} = \frac{\mathbf{p}_{i\alpha}}{m_{i\alpha}}, \quad \dot{\mathbf{p}}_{i\alpha} = \mathbf{F}_{i\alpha}^{LJ} + \mathbf{F}_{i\alpha}^{C} - \zeta_M \frac{m_{i\alpha}}{M_i}\mathbf{p}_i. \tag{17}$$

The force on a site is separated into two terms: $\mathbf{F}_{i\alpha}^{LJ}$ is the contribution due to the LJ potential interactions and $\mathbf{F}_{i\alpha}^{C}$ is the constraint force for the FJC system. ζ_M is the molecular thermostat multiplier. For butane the EOM are

$$\dot{\mathbf{r}}_{i\alpha} = \frac{\mathbf{p}_{i\alpha}}{m_{i\alpha}}, \quad \dot{\mathbf{p}}_{i\alpha} = \mathbf{F}_{i\alpha}^{T} + \mathbf{F}_{i\alpha}^{C} - \zeta_M \frac{m_{i\alpha}}{M_i}\mathbf{p}_i, \tag{18}$$

where $\mathbf{F}_{i\alpha}^{T}$ represents the total force due to potential interactions and dihedral forces, and $\mathbf{F}_{i\alpha}^{C}$ represents the intramolecular constraint forces. The EOM and the procedure for determining constraint forces for butane are outlined in [30]. The molecular thermostat multiplier which is derived from Gauss' principle of least constraint and acts to keep the molecular center of mass kinetic temperature T_M constant is given by [47]

$$\zeta_M = \frac{\sum_{i=1}^{N_m} \mathbf{F}_i \cdot \mathbf{p}_i / M_i}{\sum_{i=1}^{N_m} \mathbf{p}_i^2 / M_i}. \tag{19}$$

The molecular temperature T_M is defined by

$$T_M = \frac{1}{(dN_m - N_c)k_B} \left\langle \sum_{i=1}^{N_m} \frac{\mathbf{p}_i^2}{m_i} \right\rangle, \tag{20}$$

where angled brackets denote an ensemble average, d is the dimensionality of the system, and $N_c=4$ is the number of constraints on the molecular center of mass degrees of freedom (i.e., constraints on the center of mass momenta and kinetic energy). We will not distinguish between atomic and molecular temperature but simply use T to indicate the temperature. The details of the constraint algorithm have been discussed previously [30,48–50]. A sparse matrix linear equation solver is also used for the FJC system [51].

C. Simulation details

After the initial equilibration, we performed production runs for a minimum of 1.4×10^7 time steps averaging 14 runs each of length 10^6 steps. The transverse momentum density ACFs were computed over at least ten reduced time units for 10-site molecules and over at least 20 reduced time units for 50-site molecules. The stress ACFs were computed over at least 20 and 40 reduced time units for 10-site and 50-site molecules, respectively. Both, the transverse momentum density and stress ACFs were computed at wave vectors $k_{yn}=2\pi n/L_y$, where mode number n is from 0 to 40 with increment of 2 and $L_y=(N_a/\rho)^{1/3}$. For the remainder of this paper we drop the n index in k_{yn} for simplicity. The ACFs were Laplace transformed with respect to time using Filon's rule [47], and the wave-vector- and frequency-dependent viscosities were calculated using Eqs. (8) and (12). Equation (8) was used to obtain the wave-vector viscosities at nonzero wave vector and Eq. (12) was used to obtain the zero wave-vector viscosity.

IV. RESULTS AND DISCUSSION

The results presented below have been obtained by simulation of 108 and 864 molecules in the isokinetic molecular-dynamics ensemble. In this section we report results for transverse momentum density and shear stress autocorrelation functions, structural properties, reciprocal and real space viscosity kernels for two molecular systems, namely, butane and FJC polymeric melts. In order to validate our code and results we reproduced and compared previous results for correlation functions, self-diffusion and zero wave vector, zero frequency-dependent viscosities of butane and FJC chains where possible. Very good agreement was found in all cases.

A. Correlation functions

Initially, we examine the momentum density and shear stress autocorrelation functions in atomic and molecular representations. We must first note that the ACFs were evaluated for both 108 and 864 molecule systems in order to determine whether the results were system size dependent. No such evidence was found for butane as well as for FJC systems. In order to limit the number of figures, we only display the results for one state point for butane and FJC molecules and for system size $N_m=864$.

The transverse momentum density ACFs in atomic and molecular representations for four nonzero wave-vectors are shown for butane in Figs. 1(a) and 1(b) and for FJC in Figs. 2(a) and 2(b). Their corresponding integrals are shown in Figs. 1(c), 1(d), 2(c), and 2(d) respectively. The general features of our transverse momentum density ACFs are in agreement with those observed previously for hard spheres [12] and for Lennard Jones liquids [17]. Though the simulated values of $C_\perp(k_{y2},t=0)$ [for butane $C_\perp(k_{y2}, t=0)=5.913$ at $\rho=1.46$, $T=4.05$] in the molecular representation are in agreement with theoretical values [Eq. (11)] [for butane $C_\perp(k_{y2}, t=0)=5.909$, $\rho=1.46$, $T=4.05$], a closer examination of Figs. 1(a) and 2(a) shows that, in the atomic representation, the zero time momentum density ACFs differ for different k_y values. Presumably, this is a consequence of correlations between the momenta of different sites on the same molecule that are involved in bond angle or bond length constraints [see Evans and Morriss, Chap. 4, Eq. (37) in [13]]. As a consequence, there is no longer a simple relationship between the temperature and the zero time value of the momentum density ACF. This is confirmed by the following analysis.

Having the transverse momentum current for a molecular system in the atomic representation defined by Eq. (3), we can form the equilibrium transverse current autocorrelation function by

$$\langle J_x(k_y) J_x^*(k_y)\rangle = \left\langle \sum_{i=1}^{N_m}\sum_{\alpha=1}^{N_s} p_{xi\alpha} e^{ik_y y_{i\alpha}} \sum_{j=1}^{N_m}\sum_{\beta=1}^{N_s} p_{xj\beta} e^{-ik_y y_{i\beta}} \right\rangle. \tag{21}$$

If we expand Eq. (21) into

$$\begin{aligned}\langle J_x(k_y) J_x^*(k_y)\rangle = &\left\langle \sum_{i=1}^{N_m}\sum_{\alpha=1}^{N_s} p_{xi\alpha}^2 \right\rangle \\ &+ \left\langle \sum_{i=1}^{N_m}\sum_{\alpha=1}^{N_s}\sum_{\beta\neq\alpha}^{N_s} p_{xi\alpha} p_{xi\beta} e^{ik_y(y_{i\alpha}-y_{i\beta})} \right\rangle \\ &+ \left\langle \sum_{i=1}^{N_m}\sum_{\alpha=1}^{N_s}\sum_{j\neq i}^{N_m}\sum_{\beta=1}^{N_s} p_{xi\alpha} p_{xj\beta} e^{ik_y(y_{i\alpha}-y_{j\beta})} \right\rangle,\end{aligned} \tag{22}$$

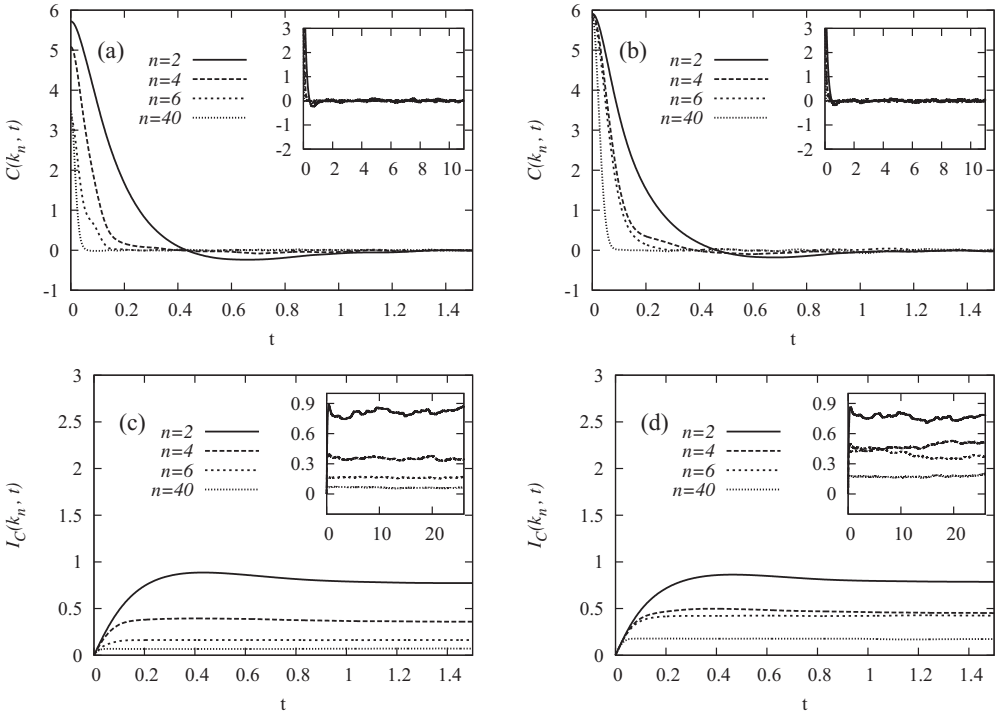

FIG. 1. Momentum density ACFs as a function of mode number n for butane in atomic and molecular formalisms (ρ=1.46, T=4.05, N_m=864, and N_s=4): (a) atomic transverse momentum density ACFs [Eq. (9)]; (b) molecular transverse momentum density ACFs [Eq. (9)]; (c) integral of the atomic transverse momentum density ACFs [Eq. (10)]; (d) integral of the molecular transverse momentum density ACFs [Eq. (10)]. The insets show the long-time behaviors for the same mode numbers.

we can see that Eq. (22) factorizes into three terms. The first term is the total atomic kinetic energy, which is directly related to the atomic temperature. The second term involves the zero time value of a correlation function of the momenta for different atoms on the same molecule. These atoms may be connected by constraints and their momenta will be cor-

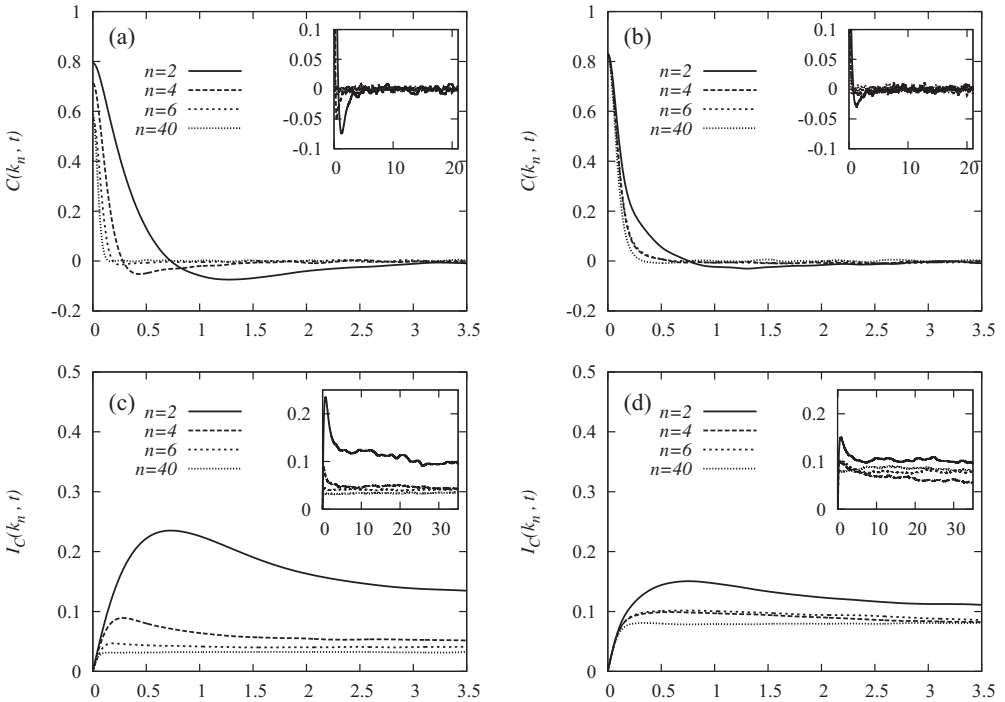

FIG. 2. Momentum density ACFs as a function of mode number n for FJC in atomic and molecular formalisms (ρ=0.84, T=1.0, N_m=108, and N_s=10): (a) atomic transverse momentum density ACFs [Eq. (9)]; (b) molecular transverse momentum density ACFs [Eq. (9)]; (c) integral of the atomic transverse momentum density ACFs [Eq. (10)]; (d) integral of the molecular transverse momentum density ACFs [Eq. (10)]. The insets show the long-time behaviors for the same mode numbers.

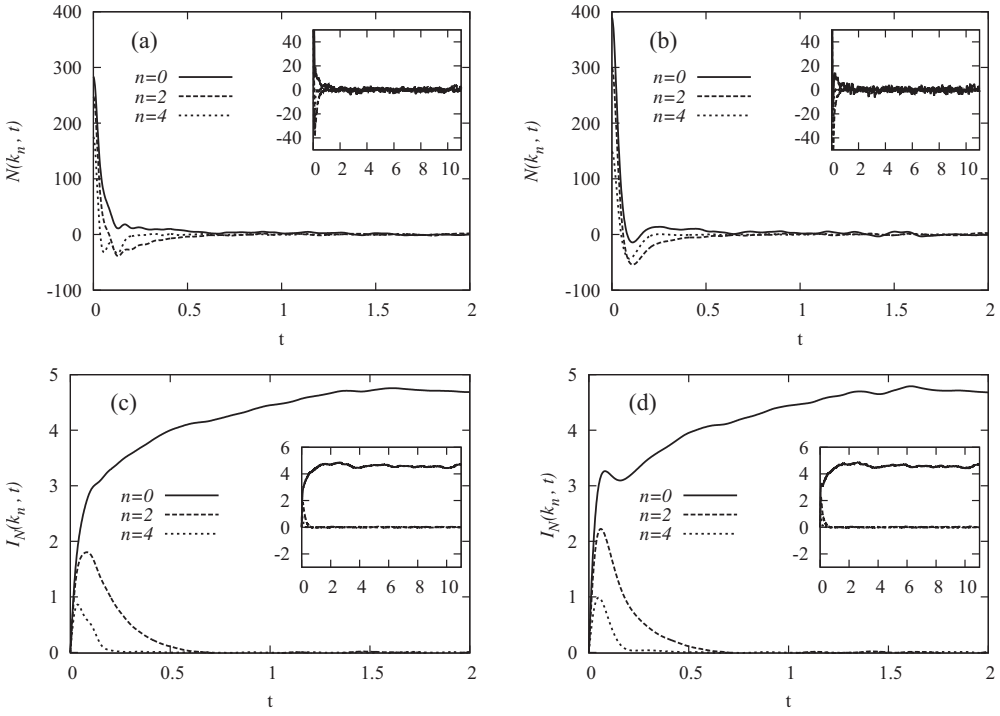

FIG. 3. Stress ACFs as a function of mode number n for butane in atomic and molecular formalisms ($\rho=1.46$, $T=4.05$, $N_m=864$, and $N_s=4$): (a) atomic stress ACFs [Eq. (13)]; (b) molecular stress ACFs [Eq. (13)]; (c) integral of the atomic stress ACFs [Eq. (15)]; (d) integral of the molecular stress ACFs [Eq. (15)]. The insets show the long-time behaviors for the same mode numbers.

related, so the mean value of this term is expected to have a nonzero value. The third term, involving correlations between the momenta of atoms on different molecules is expected to be zero at equilibrium. Therefore the y intercepts in Figs. 1 and 2 are computed from the correlation function in Eq. (9) and not from the temperature [Eq. (11)].

The shear stress ACFs in atomic and molecular representations for four wave vectors are plotted for butane in Figs. 3(a) and 3(b) and for FJC in Figs. 4(a) and 4(b) and their integrals in Figs. 3(c), 3(d), 4(c), and 4(d) respectively. All the ACFs show a fast oscillatory initial decay followed by a long-time tail. The tail's noise is surprisingly higher in the molecular formalism and equally pronounced in both butane and polymeric systems. The main difference between zero and finite k_y functions is that their time integral is proportional to the viscosities at $k_y=0$, but it vanishes for nonzero k_y due to the conservation law. As a consequence the generalized viscosities cannot be obtained from the Green-Kubo integration at nonzero k_y as pointed out by Evans and Morriss [13]. The long-time value of the zero wave-vector integral (the Green-Kubo expression for the viscosity) converges to a viscosity of 4.8 for butane, which is in excellent agreement with the Green-Kubo data at the same state point given by Daivis and Evans [52]. The butane system shows a shorter convergence time value compared to polymeric systems.

B. Reciprocal space viscosity kernel

The reciprocal space viscosity kernels for model butane and FJC are shown in Figs. 5–7. The error bars are within the symbol sizes and are therefore omitted. The statistical reliability of reciprocal space kernel data increases as k_y increases.

For butane we found the zero wave-vector zero frequency viscosity to be $\eta_0=4.8\pm0.2$ which agrees with the results of Daivis *et al.* [52] 4.8 ± 0.1 (or 0.154 ± 0.004 kg m^{-1} s^{-1}). For polymer melts we found $\eta_0=8.1\pm0.2(N_s=10)$, $\eta_0=15.2\pm0.3(N_s=20)$, and $\eta_0=41.2\pm0.4(N_s=50)$ which agrees with the limiting values $\eta_0=8.42\pm0.04(N_s=10)$, $\eta_0=15.6\pm0.1(N_s=20)$, and $\eta_0=41.3\pm0.6(N_s=50)$ [42] of the shear viscosities at zero strain rate. Kröger *et al.* also reported a slightly lower viscosity of 7.09 ± 0.09 for a 10-site FENE (finite extensible nonlinear elastic) chain [43]. We see that the zero wave-vector viscosity follows a simple proportionality $\eta\propto N_s$ (typically described by a Rouse model) which confirms that the chain considered here is not long enough to cover the crossover regime from the nonentangled to the entangled state.

In Figs. 5(a) and 5(b) we compare the reciprocal space kernels of butane at two state points ($\rho=1.46$, $T=4.05$) and ($\rho=1.46$, $T=3.79$). While the zero wave-vector viscosity decreases with temperature from 5.41 at $T=3.79$ to 4.76 at $T=4.05$, the width and the shape of the normalized kernel data varies insignificantly in this range of temperatures getting slightly larger at $T=4.05$. The kernel data points in Figs. 5(a) and 5(b) have also been fitted to several functional forms identified previously for simple monatomic and diatomic fluids [15,16]. We discuss the parametrization of the reciprocal space kernels further below. In Fig. 6 we plot the wave-vector dependent viscosity for a polymeric chain upon increasing the chain length. It is seen that the zero wave-vector viscosity increases linearly

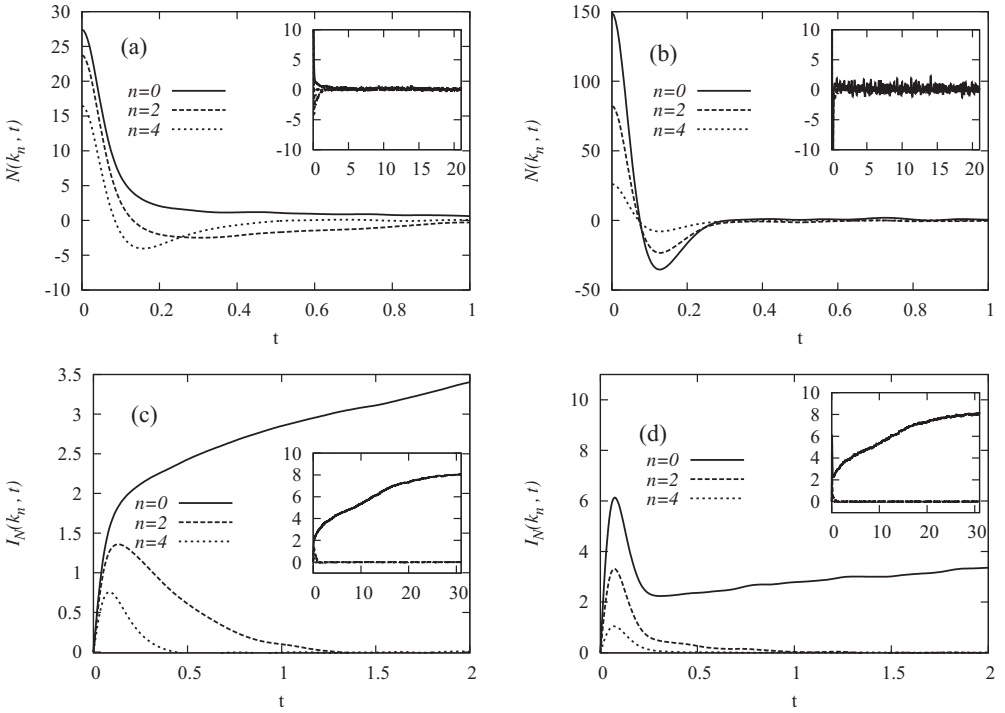

FIG. 4. Stress ACFs as a function of mode number n for FJC in atomic and molecular formalisms (ρ=0.84, T=1.0, N_M=108, and N_s=10): (a) atomic stress ACFs [Eq. (13)]; (b) molecular stress ACFs [Eq. (13)]; (c) integral of the atomic stress ACFs [Eq. (15)]; (d) integral of the molecular stress ACFs [Eq. (15)]. The insets show the long-time behaviors for the same mode numbers.

with N_s. However, the half width at half maximum is almost constant which suggests that the normalized shape of the reciprocal space kernel with respect to zero wave-vector value must be identical for all three chain lengths. Further evidence supporting this statement will be shown later in Fig. 7.

For completeness we also compared the FJC kernels with kernels computed for FENE [43] chain systems of equivalent

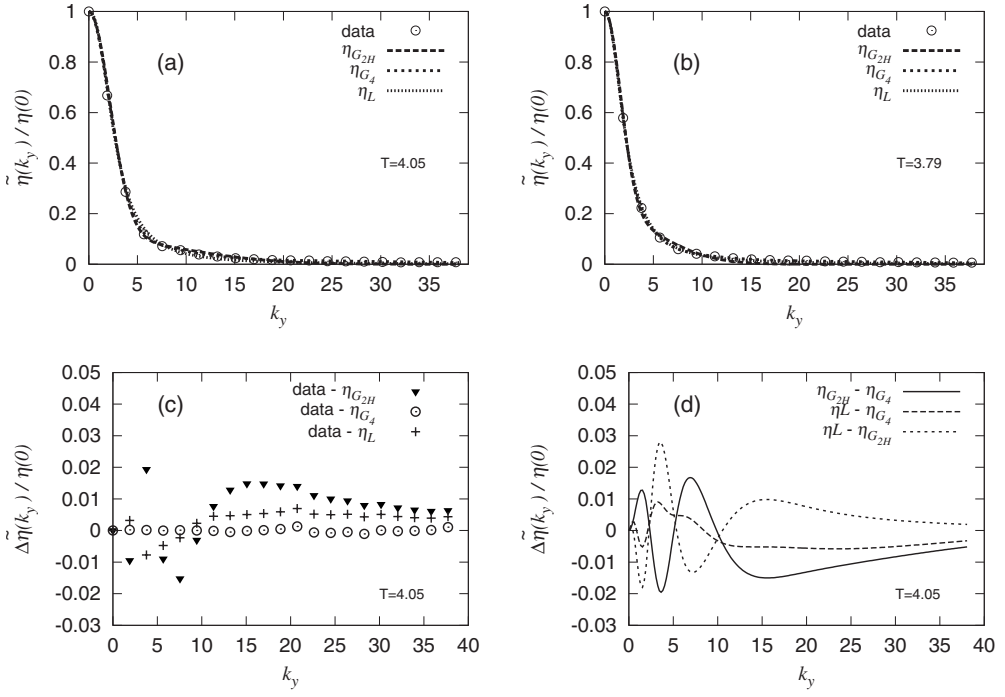

FIG. 5. Reciprocal space kernel of butane (ρ=1.46, N_m=864) in the atomic formalism: (a) normalized kernel data at T=4.05 and best fits to Eqs. (23) and (24); (b) normalized kernel data at T=3.79 and best fits to Eqs. (23) and (24); (c) Differences between the kernel data and fits shown in (a); (d) Differences between the fits shown in (a).

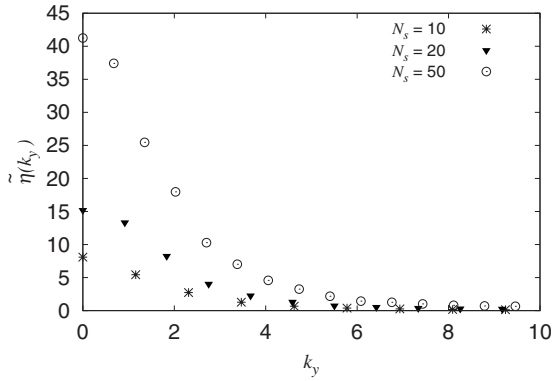

FIG. 6. Reciprocal space kernel of FJC melts in the atomic formalism at three different chain lengths (ρ=0.84, T=1.0, and N_m=864).

molecular weight and state point. The kernels in both models were essentially identical, therefore FENE results are not explicitly displayed in this paper. The similarity of the viscosity kernel of these two molecules arises because, despite using different algorithms, the molecular structure varies only slightly. The similarity of FJC and FENE systems has also been recently confirmed by Hunt and Todd [53,54] for shear and extensional viscosities and diffusion tensor. The computational efficiency of the FENE and FJC force calculations are also similar due to the sparse matrix linear equation solver used for tridiagonal matrices which is applied in the FJC system [55,56].

As one parameter functional forms that fit the data in both low and high k_y regions could not be found in our previous attempts for atomic and diatomic systems [15,16], we here present only the best fits with two or more fitting parameters. Particularly we tested two functional forms: a N_G term Gaussian function

$$\tilde{\eta}_G(k_y) = \eta_0 \sum_j^{N_G} A_j e^{-k_y^2/2\sigma_j^2} \quad A_j, \sigma_j \in \mathbb{R}_+ \tag{23}$$

and a Lorentzian type function

$$\tilde{\eta}_L(k_y) = \frac{\eta_0}{1 + \alpha |k_y|^\beta} \quad \alpha, \beta \in \mathbb{R}_+. \tag{24}$$

We present the best fits of the data to (i) a two-term Gaussian function with freely estimated amplitudes (i.e., unconstrained fitting) termed as $\tilde{\eta}_{G_2}$, (ii) to a two-term Gaussian function with interdependent amplitudes (i.e., constrained fitting $\Sigma_j^{N_G} A_j = 1$) given by Hansen *et al.* [15] and termed as $\tilde{\eta}_{G_{2H}}$, (iii) to a four-term Gaussian function with freely estimated amplitudes, termed as $\tilde{\eta}_{G_4}$, and (iv) to the Lorentzian type function [Eq. (24)]. In order to measure the magnitude of the residuals we use the residual standard deviation defined as $s_r = \sqrt{\Sigma_{n=1}^{n_s} r^2/(n_s - n_p)}$, where n_s is the number of data points, n_p is the number of fitting parameters, and r is the residual

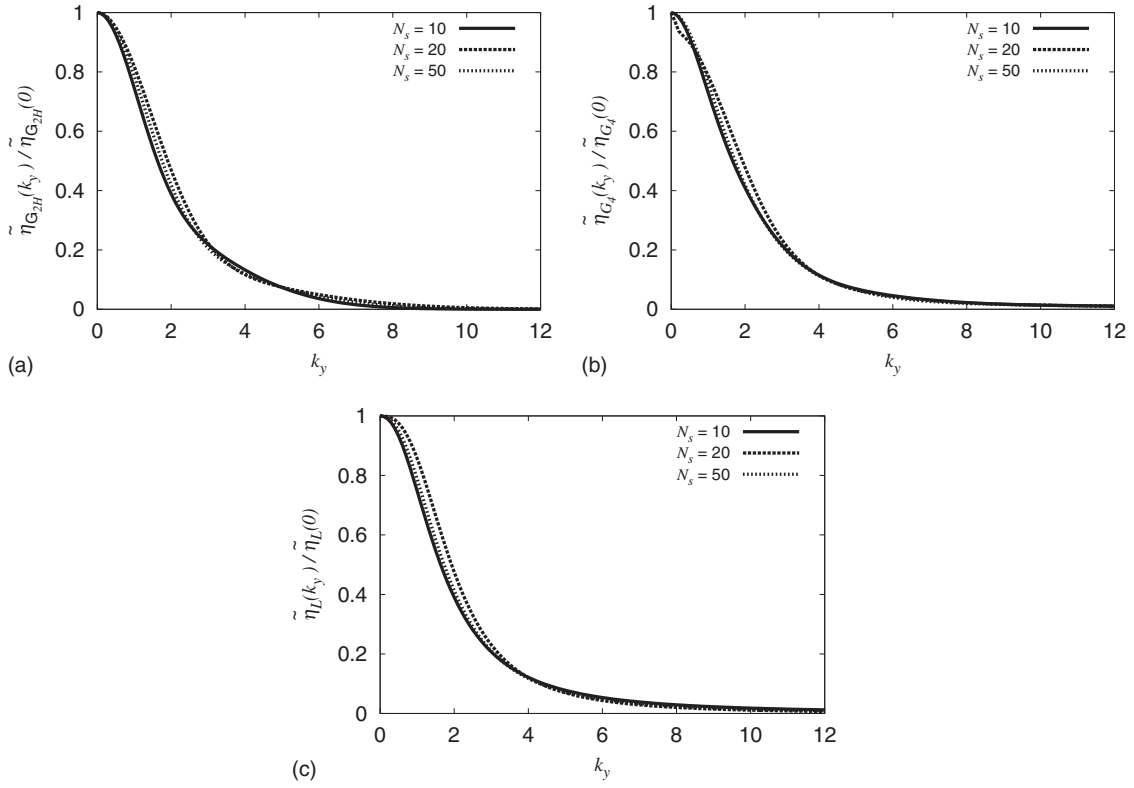

FIG. 7. Normalized reciprocal space kernels of FJC melts at three different chain lengths: N_s=10, N_s=20, and N_s=50 (ρ=0.84, T=1.0, and N_m=864): (a) kernels obtained from the two-term Gaussian functional form (23); (b) kernels obtained from the four-term Gaussian functional form (23); (c) kernels obtained from the Lorentzian-type functional form (24).

TABLE II. Zero-frequency, zero wave-vector shear viscosity, and fitting parameter values for molecular systems in atomic representation.

		Butane			FJC	
State Point	ρ	1.46	1.46		0.84	
	T	4.05	3.79		1.0	
System size	N_m	864			864	
	N_s	4		10	20	50
	η_0	4.8[0.2][a]	5.4[0.3]	8.1[0.2]	15.2[0.3]	41.2[0.4]
Two-term Gaussian, $A_2=1-A_1$ Eq. (23)	A	0.133	0.202	0.375	0.170	0.250
	σ_1	10.29	6.708	2.769	3.810	3.213
	σ_2	2.105	1.585	1.044	1.452	1.261
	s_r	0.078	0.086	0.092	0.194	0.552
Two-term Gaussian Eq. (23)	A_1	0.123	0.200	0.368	0.139	0.252
	A_2	0.855	0.795	0.629	0.842	0.749
	σ_1	10.87	6.764	2.792	4.169	3.203
	σ_2	2.170	1.598	1.056	1.511	1.257
	s_r	0.077	0.089	0.094	0.181	0.567
Four-term Gaussian Eq. (23)	A_1	0.646	0.349	0.571	0.773	0.544
	A_2	0.231	0.532	0.270	0.061	0.188
	A_3	0.094	0.095	0.144	0.147	0.251
	A_4	0.028	0.023	0.016	0.019	0.027
	σ_1	2.549	2.762	1.618	1.556	1.413
	σ_2	1.127	1.284	0.730	0.093	0.811
	σ_3	7.876	7.175	3.423	3.227	2.639
	σ_4	28.17	28.02	12.92	11.29	8.544
	s_r	0.006	0.004	0.006	0.102	0.443
Lorentzian-type Eq. (24)	α	0.145	0.235	0.338	0.167	0.270
	β	1.997	1.872	2.210	2.726	2.398
	s_r	0.046	0.032	0.054	0.069	0.417

[a]Numbers in square brackets represent standard errors of the mean.

[57]. After an iterative curve fitting procedure the accurate estimation of η_0 was kept fixed allowing all other parameters in Eqs. (23) and (24) to be used as fitting parameters. In Table II we have listed the fitting parameters for our molecular systems. Table III also confirms the value of 1 for the total Gaussian amplitudes.

The results show that a relatively simple equally weighted two-term Gaussian function fits the butane data [Figs. 5(a) and 5(b)] with less than 2% error [Fig. 5(c)]. The Lorentzian-type function fits the butane data much better over the entire wave-vector range. While generally a third term in the Gaussian function improves the fit, only the fourth term shows a better precision compared to the Lorentzian-type function, Fig. 5(c). In Fig. 5(d) we plot the differences between all three functional forms for the same state point of butane. It is seen that the difference between the four-term Gaussian and Lorentzian-type function is less than 1% and either one of these two should be preferred. It is obvious that eight parameters makes the four-term Gaussian expansion of the reciprocal space kernel less convenient but on the other hand, the Gaussian function can be analytically inverse Fourier transformed while the inverse Fourier transform of the Lorentzian-type function can in general only be evaluated numerically.

TABLE III. Total amplitude for Gaussian functional form.

		Butane			FJC	
State Point	ρ	1.46	1.46		0.84	
	T	4.05	3.79		1.0	
	N_s	4		10	20	50
Two-term Gaussian	$\Sigma_{j=1}^{2}A$	0.978	0.995	0.997	0.981	1.001
Four-term Gaussian	$\Sigma_{j=1}^{4}A$	0.997	0.999	1.001	1.000	0.940

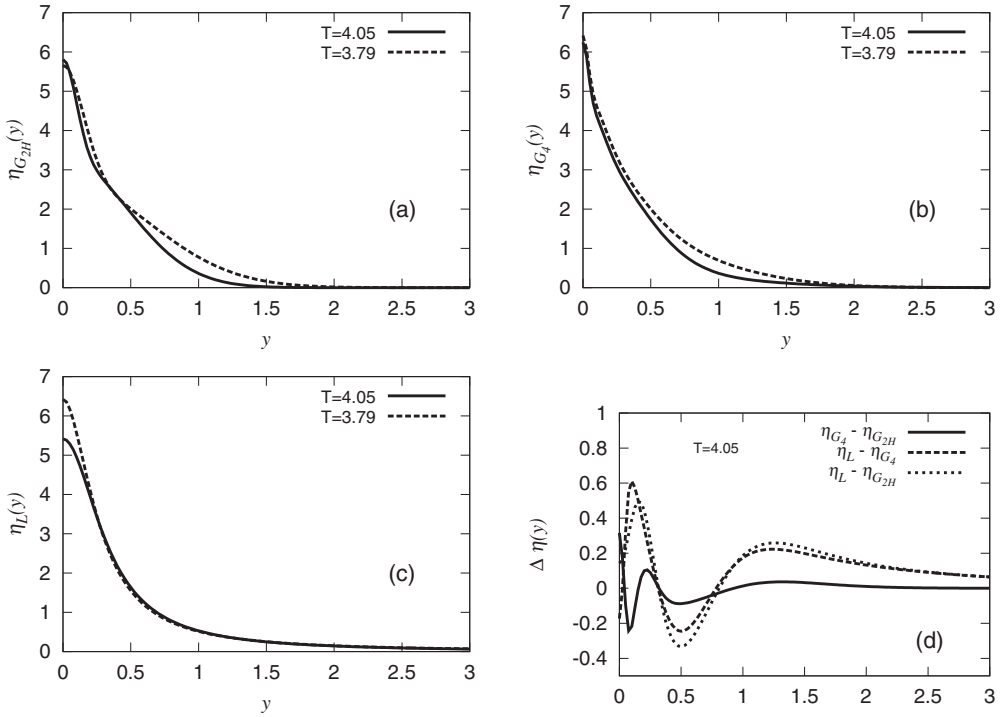

FIG. 8. Real-space kernel of butane (ρ=1.46) at two different temperatures, T=4.05 and T=3.79: (a) real-space kernels obtained from the two-term Gaussian functional form Eq. (26); (b) real-space kernels obtained from the four-term Gaussian functional form Eq. (26); (c) real-space kernels obtained numerically from the Lorentzian-type functional form Eq. (24); (d) difference between the kernels (a)–(c) for T=4.05.

In Figs. 7(a)–7(c) we plot the Gaussian and Lorentzian-type fits to the atomic reciprocal space kernel data of the FJC system shown previously in Figs. 6 at three different chain lengths. Though the shape of the normalized kernels is slightly affected by the choice of fitting function it shows very little difference upon increase in the chain length. Essentially, the normalized reciprocal space kernel of polymer melts does not change with the chain lengths considered here and the insignificant deviations could simply be due to the numerical error of the fitting procedure and relatively high zero wave-vector value the reciprocal space kernels are normalized with as we increase the chain length.

C. Real-space viscosity kernel

The viscosity kernel in physical space can be found via an inverse Fourier cosine transform, $F_c^{-1}[\ldots]$ which is a special case of the continuous Fourier transform of even functions. The viscosity kernel in reciprocal space is an even function (it is symmetric about the origin) consequently the real space kernel is symmetric because the Fourier transform preserves the even properties of the function to be transformed. Since the integral is being computed over an interval symmetric about the origin (i.e., $-\infty$ to $+\infty$), the second integral must vanish to zero, and the first may be simplified to give

$$F_c^{-1}[\tilde{\eta}(k_y)] = \eta(y) = \sqrt{\frac{2}{\pi}}\int_0^\infty \tilde{\eta}(k_y)\cos(k_y y)dk_y. \quad (25)$$

The inverse Fourier cosine transform of the Gaussian function [Eq. (23)] exists [58], and it is even possible to obtain an analytical expression. For an N_G term Gaussian function the inverse Fourier cosine transform is

$$\eta_G(y) = \frac{\eta_0}{\sqrt{2\pi}}\sum_j^{N_G} A_j\sigma_j \exp[-(\sigma_j y)^2/2] \quad A_j,\sigma_j \in \mathbb{R}_+. \quad (26)$$

For the Lorentzian-type function, the integral in Eq. (25) was evaluated numerically by a Simpson method [15,16].

The real-space viscosity kernel results for butane at two temperatures (T=4.05 and T=3.79) are presented in Fig. 8 and data for polymer melts at three densities are presented in Fig. 9. The real-space kernel decreases slightly with the temperature, but it is strongly affected by the choice of fitting function in reciprocal space. For instance, kernels obtained from a two-term equally weighted Gaussian functional form, shown in Fig. 8(a), are strongly distorted in physical space and therefore more terms in the Gaussian form are needed. To illustrate this point, we consider a four-term Gaussian shown in Fig. 8(b). Kernels obtained numerically from the Lorentzian-type functional form are shown in Fig. 8(d) and feature a much smoother behavior in real space. The maximum difference between the kernels obtained from the Gaussian functions is about 5% and between the kernels obtained from the Lorentzian-type function and Gaussian functions is less than 10% [Fig. 8(d)].

For the FJC system, the trends are illustrated in Fig. 9 for un-normalized data and in Fig. 10 for normalized data. The difference between these functional forms is given in Fig. 11. Despite the very large discrepancy between kernels predicted

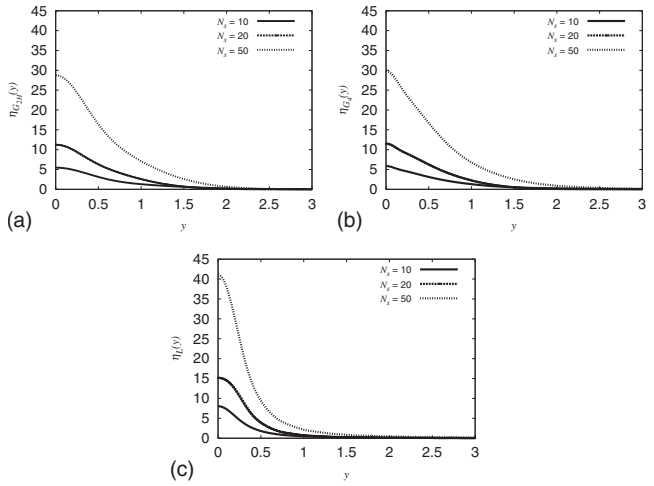

FIG. 9. Real-space kernel of FJC melts at three different chain lengths $N_s=10$, $N_s=20$, and $N_s=50$ ($\rho=0.84$, $T=1.0$, and $N_m=864$): (a) real-space kernels obtained from the equally weighted two-term Gaussian functional form Eq. (26); (b) real-space kernels obtained from the four-term Gaussian functional form Eq. (26); (c) real-space kernels obtained numerically from the Lorentzian-type functional form Eq. (24).

by a four-term Gaussian function and a Lorentzian-type function of almost 40% at $y=0$ [Fig. 11(a)], the local effective viscosity, η_0, obtained by integrating the nonlocal real space kernel over y is in good agreement. As mentioned previously, the four-term Gaussians show much better fits and must be trusted when transforming the reciprocal space kernels to physical domain. However, we note that the four-term Gaussian function is sensitive to outliers and may result in unnatural behavior while the Lorentzian-type function shows a much smoother shape of the real-space kernels.

The zero wave-vector viscosity η_0 obtained via a Gaussian function $\eta_G(y)$ is

$$\eta_0 = \int_{-\infty}^{\infty} \eta_G(y)dy = \frac{\eta_0}{\sqrt{2\pi}} \int_{-\infty}^{\infty} \left\{ \sum_{j}^{N_G} A_j \sigma_j \exp[-(\sigma_j y)^2/2] \right\} dy, \tag{27}$$

where $N_G=2$ for the two-term Gaussian and $N_G=4$ for the four-term Gaussian. The difference between the kernels ob-

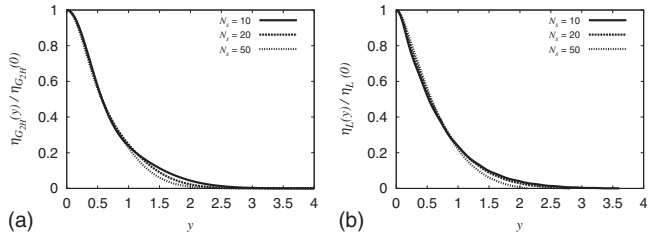

FIG. 10. Real-space kernel of FJC melts at three different chain lengths, $N_s=10$, $N_s=20$, and $N_s=50$ ($\rho=0.84$, $T=1.0$, and $N_m=864$): (a) real-space kernels normalized by $\eta(y=0)$ value obtained from the equally weighted two-term Gaussian functional form Eq. (26); (b) real-space kernels normalized by $\eta(y=0)$ value and obtained numerically from the Lorentzian-type functional form Eq. (24).

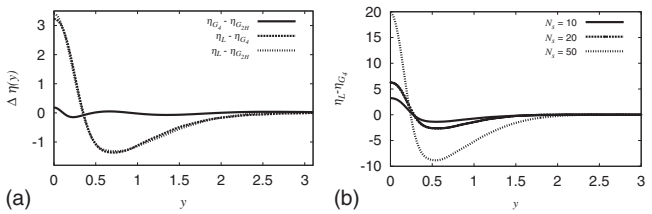

FIG. 11. Difference between the real space kernels for (a) 10-site FJC system obtained from three functional forms and (b) the difference between the real space kernels obtained from the Lorentzian-type and four-term Gaussian functions for three different chain lengths N_s.

tained from the Lorentzian-type function and the four-term Gaussian functions increases with the chain length [Fig. 11(b)]. However, the local effective viscosities agree with the computed values even at high molecular weights.

The numerical results from all three functional forms are shown in Table IV. Though all three functional forms yield different kernel shapes, the local effective viscosities η_0 are in good agreement with the simulated values presented in Table II. It is seen that the error associated with the integration is less than 2% compared to simulated zero frequency zero wave-vector viscosities given in Table II. This confirms the accuracy of our numerical analysis.

In order to compare the real-space viscosity kernels for different molecular systems we define a normalization factor that accounts for the structural properties [16]

$$\xi_g = \frac{\int_0^{\infty} r[g(r)-1]^2 dr}{\int_0^{\infty} [g(r)-1]^2 dr}, \tag{28}$$

where ξ_g is a measure of the range over which the correlation function decays to 1 and therefore could be regarded as a correlation length of the radial distribution function (RDF). The RDF is calculated either in terms of the distance vector between atoms i and j or between the centers of mass of molecules i and j: $g(r)=\langle \frac{\Sigma_{i=1}^{N}\Sigma_{j>1}^{N}\delta(|\mathbf{r}-\mathbf{r}_{ij}|)}{4\pi r^2 N\rho} \rangle$. N is the total number of molecules or atoms and ρ is the atomic or molecular number density. The RDF gives us important information about structure in dense liquid butane and polymer melts and corresponding normalization factors for these systems are presented in Fig. 12.

RDFs for butane at state point ($\rho=1.46$, $T=4.05$) and ($\rho=1.46$, $T=3.79$) are shown in Fig. 12 and have the same form as those from [30,33]. The sharp peaks at $\sigma=0.39$ and $\sigma=0.63$ arising from nearest- and next-nearest-neighbor constraints are omitted from the calculation of ξ_g in Eq. (28). The broad and sharp peaks in Figs. 12(a) and 12(b) correspond to *gauche* and *trans* conformations respectively. The remainder of the $g(r)$ curves shows intermolecular correlations. For the FJC system the radial distribution functions, given for $N_s=10$, $N_s=20$, and $N_s=50$ in Figs. 12(c)–12(e) show the sharp peaks due to bonds ($l=1.0\sigma$) and LJ shells. The second LJ coordination shell is visible in a peak at $r \approx 2\sigma$. Our RDF for polymer melts are in agreement with

TABLE IV. Effective viscosities evaluated from $\eta_{G_{2H}}(y)$, $\eta_{G_4}(y)$, and numerically from $\eta_L(k_y)$.

		Butane			FJC	
State Point	ρ	1.46	1.46		0.84	
	T	4.05	3.79		1.0	
System size	N_m	864			108	
	N_s	4		10	20	50
Two-term Gaussian	η_0	4.759	5.410	8.09	15.2	41.2
Four-term Gaussian	η_0	4.760	5.410	8.09	15.2	41.2
Lorentzian	η_0	4.761	5.412	8.09	15.2	41.2

[59,60]. Compared to butane, for which ξ_g changes significantly from 0.489 at state point $\rho=1.676$, $T=4.05$ to 1.195 at state point $\rho=1.46$, $T=3.79$, ξ_g for FJC only slightly increases from 0.534 to 0.548 as we enlarge the polymers from 10 to 50 sites per molecule.

The real-space kernels for butane, normalized with respect to their zero wave-vector values and spatial scaling factor ξ_g are shown in Fig. 13. First, we see that the kernel obtained from a Lorentzian-type fit for two different temperatures $T=4.05$ (continuous line) and $T=3.79$ (long-dashed line) [Fig. 13(b)] normalized with respect to ξ_g deviate substantially from their un-normalized analogs shown in Fig. 13(a). Since the normalization factor has been calculated from the total intramolecular and intermolecular radial distribution function it is to be expected that the peaks due to intramolecular interactions will have a greater contribution at low temperatures as seen in Fig. 13(b). Therefore, in addition to previously given kernels, we also plot the normalized kernels with respect to only the intermolecular RDF [dashed and dotted lines in Fig. 13(b)]. We can see that the kernels are closer in Fig. 13(b) for the same set of temperatures and densities. However, our normalization did not remove the discrepancy between the kernels for these two structures, i.e., at $T=4.05$ (dashed line) and $T=3.79$ (dotted line).

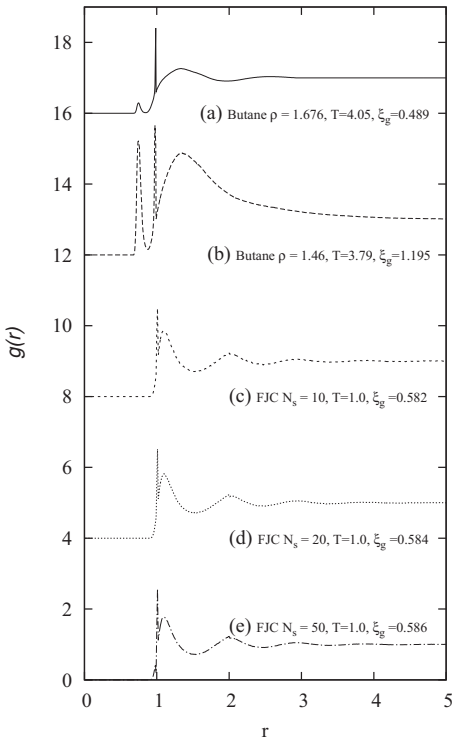

FIG. 12. Total intramolecular and intermolecular radial distribution function $g(r)$ and normalization factors ξ_g for butane at two state points (a) ($\rho=1.46$, $T=4.05$), (b) ($\rho=1.46$, $T=3.79$) and FJC at state point ($\rho=0.84$, $T=1.0$, and $N_m=864$) for (c) $N_s=10$, (d) $N_s=20$, and (e) $N_s=50$. For butane the peaks at $\sigma=0.30$ and $\sigma=0.63$ arising from nearest-neighbor and next-nearest neighbor constraints are omitted. For clarity, the RDFs in (d), (c), (b), and (a) are shifted upwards by four units.

Figures 14(a) and 14(b) depict the FJC kernels in physical space according to the atomic definition, normalized with respect to ξ_g and obtained from an equally weighted two-term Gaussian function and Lorentzian-type function, respectively. We can see that despite the fact that the structural normalization procedure preserved the features of the real space kernels, neither Lorentzian-type function nor Gaussian function completely remove the differences between the kernels in Figs. 10(a) and 10(b). As mentioned above for butane, a more comprehensive structural normalization is needed in order to be able to reduce the viscosity kernels to a universal curve for complex molecular fluids.

V. CONCLUSION

We have computed the wave-vector-dependent viscosities and their inverse Fourier transforms for two molecular systems: butane and linear FJC chains. Agreement between our results and other equilibrium data in the zero-frequency zero

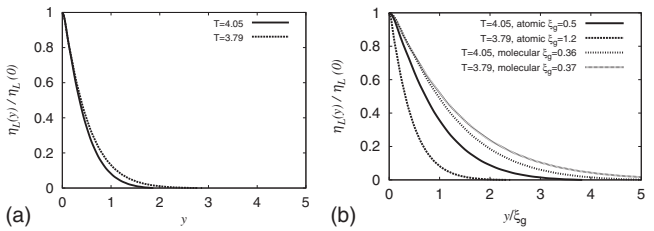

FIG. 13. Real-space kernel of butane ($\rho=1.46$) obtained in the atomic formalism at two different temperatures, $T=4.05$ and $T=3.79$: (a) real-space kernels in the atomic formalism obtained from the Lorentzian-type functional form and normalized by $\eta(y=0)$ value; (b) real-space kernels shown in (a) normalized by the factor ξ_g. Note intermolecular interaction normalization in (b) (dotted and dashed lines).

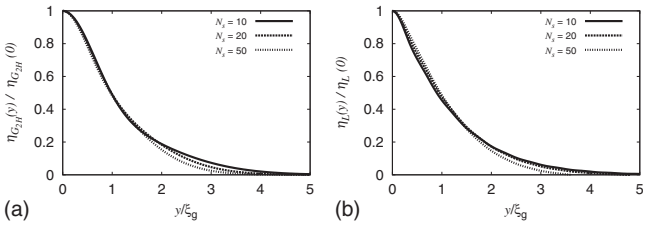

FIG. 14. Real-space kernel of FJC melts for three different chain lengths: $N_s=10$, $N_s=20$, and $N_s=50$: (a) real-space kernels obtained from the equally weighted two-term Gaussian functional form [Eq. (26)] normalized by the factor ξ_g; (b) real-space kernels obtained from the Lorentzian-type functional form normalized by the factor ξ_g [Eq. (28)]. The corresponding structurally un-normalized kernels are shown in Fig. 10.

wave-vector limit confirms our data's validity. The main results can be summarized as follows:

(i) An insignificant variation in the shape of both normalized reciprocal space and real-space kernels has been noted for the entire range of molecular weights considered here.

(ii) Though a relatively simple Lorentzian-type function fits the data well over a wide range of wave vectors, at all the state points, it is not possible to analytically inverse Fourier transform it to the spatial domain. Therefore, one may consider an expansion up to a four-term Gaussian which also gives a better accuracy compared to the Lorentzian-type function. Even though the parametrization of the reciprocal space kernel has shown that the density and temperature have a great impact on the parameters, the resulting kernels vary only slightly with those temperatures chosen here.

(iii) We identified that the choice of functional forms in reciprocal space plays a significant role in the prediction of the real-space kernel shape. For instance, in the case of butane an equally weighted two-term Gaussian function is unsuitable as it distorts the real-space kernel and underestimates the local effective viscosities which is consistent with earlier results for monatomic and diatomic fluids. However, for polymeric fluids all the fits reproduce accurately the local effective viscosities even though they have slightly different shapes.

(iv) The viscosity kernels of FENE and FJC chains are essentially the same. Much larger chains would also be worth considering in the future in order to cover the crossover regime from the nonentangled to the entangled state.

(v) Though a normalization scaling based on the correlation length of the radial distribution function allows us to compare the real-space kernels of different polymeric melts, in the case of butane, only the intermolecular contributions in the radial distribution function leads to an improved agreement. This suggests a need for a more comprehensive structural normalization of complex molecular structures.

(vi) Overall, we have shown that the real-space viscosity kernel of butane has a width of roughly 3–5 atomic diameters while for polymer melts the width is about 4–6 atomic diameters. This means that the generalized hydrodynamic viscosity must be used in predicting the flow properties of molecular fluids on length scales where the gradient in the strain rate is of the order of these dimensions. Consequently nonlocal constitutive equations should be invoked for a complete description of flows at molecular scales under such conditions.

Finally, this work has been concerned with a few molecular systems, but the methodology can easily be used for larger and more complex molecules with different constraint schemes or nearest-neighbor bond constraints.

[1] J. C. T. Eijkel and A. van den Berg, Microfluid. Nanofluid. **1**, 249 (2005).
[2] J. O. Tegenfeldt, C. Prinz, H. Cao, R. L. Huang, R. H. Austin, S. Y. Chou, E. C. Cox, and J. C. Sturm, Anal. Bioanal. Chem. **378**, 1678 (2004).
[3] I. Bitsanis, S. A. Somers, H. T. Davis, and M. Tirell, J. Chem. Phys. **93**, 3427 (1990).
[4] I. Bitsanis, T. K. Vanderlick, M. Tirell, and H. T. Davis, J. Chem. Phys. **89**, 3152 (1988).
[5] X. B. Nie, S. Y. Chen, and M. O. Robbins, J. Fluid Mech. **500**, 55 (2004).
[6] K. P. Travis, B. D. Todd, and D. J. Evans, Phys. Rev. E **55**, 4288 (1997).
[7] K. P. Travis and K. E. Gubbins, J. Chem. Phys. **112**, 1984 (2000).
[8] J. Zhang, B. D. Todd, and K. P. Travis, J. Chem. Phys. **121**, 10778 (2004).
[9] J. Zhang, B. D. Todd, and K. P. Travis, J. Chem. Phys. **122**, 219901 (2005).
[10] B. D. Todd, J. S. Hansen, and P. J. Daivis, Phys. Rev. Lett. **100**, 195901 (2008).
[11] B. D. Todd and J. S. Hansen, Phys. Rev. E **78**, 051202 (2008).
[12] W. E. Alley and B. J. Alder, Phys. Rev. A **27**, 3158 (1983).
[13] D. J. Evans and G. P. Morriss, *Statistical Mechanics of Nonequilibrium Liquids* (Academic Press, New York, 1990).
[14] D. Levesque and L. Verlet, Mol. Phys. **61**, 143 (1987).
[15] J. S. Hansen, P. J. Daivis, K. P. Travis, and B. D. Todd, Phys. Rev. E **76**, 041121 (2007).
[16] R. M. Puscasu, B. D. Todd, P. J. Daivis, and J. S. Hansen, J. Phys.: Condens. Matter **22**, 195105 (2010).
[17] B. J. Palmer, Phys. Rev. E **49**, 359 (1994).
[18] D. Bertolini and A. Tani, Phys. Rev. E **52**, 1699 (1995).
[19] I. P. Omelyan, I. M. Mryglod, and M. V. Tokarchuk, Condens. Matter Phys. **8**, 25 (2005).
[20] R. D. Olmsted and R. F. Snider, J. Chem. Phys. **65**, 3407 (1976).
[21] R. D. Olmsted and R. F. Snider, J. Chem. Phys. **65**, 3423 (1976).
[22] R. Edberg, G. P. Morriss, and D. J. Evans, J. Chem. Phys. **86**, 4555 (1987).
[23] M. P. Allen, Mol. Phys. **52**, 705 (1984).
[24] D. J. Evans, Mol. Phys. **32**, 1171 (1976).
[25] B. D. Todd and P. J. Daivis, Mol. Simul. **33**, 189 (2007).
[26] J. H. Irving and J. G. Kirkwood, J. Chem. Phys. **18**, 817

(1950).
[27] R. M. Puscasu, Ph.D. thesis, Swinburne University of Technology, 2010 (unpublished).
[28] J. P. Hansen and I. R. McDonald, *Theory of Simple Liquids* (Academic Press, New York, 1986).
[29] P. J. Daivis and D. J. Evans, J. Chem. Phys. **100**, 541 (1994).
[30] R. Edberg, D. J. Evans, and G. P. Morriss, J. Chem. Phys. **84**, 6933 (1986).
[31] P. J. Daivis, D. J. Evans, and G. P. Morriss, J. Chem. Phys. **97**, 616 (1992).
[32] M. L. Matin, P. J. Daivis, and B. D. Todd, Comput. Phys. Commun. **151**, 35 (2003).
[33] J. P. Ryckaert and A. Bellemans, Discuss. Faraday Soc. **66**, 95 (1978).
[34] J. P. Ryckaert and A. Bellemans, Chem. Phys. Lett. **30**, 123 (1975).
[35] S. Toxvaerd, J. Chem. Phys. **93**, 4290 (1990).
[36] H. Luo and C. Hoheisel, J. Chem. Phys. **47**, 3956 (1993).
[37] H. Luo and C. Hoheisel, J. Chem. Phys. **96**, 3173 (1992).
[38] S. Chynoweth, U. C. Klomp, and Y. Michopoulos, J. Chem. Phys. **95**, 3024 (1991).
[39] H. Luo and C. Hoheisel, J. Chem. Phys. **94**, 8378 (1991).
[40] M. G. Martin and J. I. Siepmann, J. Phys. Chem. B **102**, 2569 (1998).
[41] J. D. Weeks, D. Chandler, and H. C. Andersen, J. Chem. Phys. **54**, 5237 (1971).
[42] P. J. Daivis, M. L. Matin, and B. D. Todd, J. Non-Newtonian Fluid Mech. **147**, 35 (2007).
[43] M. Kröger, W. Loose, and S. Hess, J. Rheol. **37**, 1057 (1993).
[44] K. Kremer and G. S. Grest, J. Chem. Phys. **92**, 5057 (1990).
[45] C. W. Gear, *The Numerical Integration of Ordinary Differential Equations of Various Orders* (Argonne National Laboratory, Argonne, 1966).
[46] C. W. Gear, *Numerical Initial Value Problems in Ordinary Differential Equations* (Prentice Hall, Englewood Cliffs, NJ, 1971).
[47] M. P. Allen and D. J. Tildesley, *Computer Simulation of Liquids* (Clarendon Press, Oxford, 1989).
[48] R. Edberg, D. J. Evans, and G. P. Morriss, Mol. Phys. **62**, 1357 (1987).
[49] A. Baranyai and D. J. Evans, Mol. Phys. **70**, 53 (1990).
[50] G. P. Morriss and D. J. Evans, Comput. Phys. Commun. **62**, 267 (1991).
[51] G. H. Golub and C. F. Van Loan, *Matrix Computations* (Johns Hopkins, Baltimore, 1996).
[52] P. J. Daivis and D. J. Evans, J. Chem. Phys. **103**, 4261 (1995).
[53] T. A. Hunt and B. D. Todd, Mol. Simul. **35**, 1153 (2009).
[54] T. A. Hunt and B. D. Todd, J. Chem. Phys. **131**, 054904 (2009).
[55] M. L. Matin, P. J. Daivis, and B. D. Todd, J. Chem. Phys. **113**, 9122 (2000).
[56] M. L. Matin, P. J. Daivis, and B. D. Todd, J. Chem. Phys. **115**, 5338 (2001).
[57] R. Peck, C. Olsen, and J. Devore, *Introduction to Statistics and Data Analysis* (BrooksCole, Belmont, 2008).
[58] A. Papoulis, *The Fourier Integral and Its Applications* (McCraw-Hill, New York, 1962).
[59] M. Bulacu and E. van der Giessen, Phys. Rev. E **76**, 011807 (2007).
[60] C. Bennemann, W. Paul, K. Binder, and B. Dünweg, Phys. Rev. E **57**, 843 (1998).